

NGC 6139: a normal massive globular cluster or a first-generation dominated cluster? Clues from the light elements ^{★,★,★}

A. Bragaglia¹, E. Carretta¹, A. Sollima¹, P. Donati^{1,2}, V. D’Orazi^{3,4,5}, R.G. Gratton³, S. Lucatello³, and C. Sneden⁶

¹ INAF-Osservatorio Astronomico di Bologna, Via Ranzani 1, I-40127 Bologna, Italy

² Dipartimento di Fisica e Astronomia, Università di Bologna, viale Berti Pichat 6, I-40127 Bologna, Italy

³ INAF-Osservatorio Astronomico di Padova, Vicolo dell’Osservatorio 5, I-35122 Padova, Italy

⁴ Monash Centre for Astrophysics, School of Physics and Astronomy, Monash University, Melbourne, VIC 3800, Australia

⁵ Department of Physics and Astronomy, Macquarie University, Sydney, NSW 2109, Australia

⁶ Department of Astronomy and McDonald Observatory, The University of Texas, Austin, TX 78712, USA

ABSTRACT

Information on globular clusters (GC) formation mechanisms can be gathered by studying the chemical signature of the multiple populations that compose these stellar systems. In particular, we are investigating the anticorrelations among O, Na, Al, and Mg to explore the influence of cluster mass and environment on GCs in the Milky Way and in extragalactic systems. We present here the results obtained on NGC 6139 which, on the basis of its horizontal branch morphology, had been proposed to be dominated by first-generation stars. In our extensive study based on high resolution spectroscopy, the first for this cluster, we found a metallicity of $[Fe/H] = -1.579 \pm 0.015 \pm 0.058$ (rms=0.040 dex, 45 bona fide member stars) on the UVES scale defined by our group. The stars in NGC 6139 show a chemical pattern normal for GCs, with a rather extended Na-O (and Mg-Al) anticorrelation. NGC 6139 behaves like expected from its mass and contains a large fraction (about two thirds) of second-generation stars.

Key words. Stars: abundances – Stars: atmospheres – Stars: Population II – Galaxy: globular clusters – Galaxy: globular clusters: individual: NGC 6139

1. Introduction

Once considered as a good example of simple stellar populations, Galactic globular clusters (GCs) are currently thought to have formed in a complex chain of events, which left a fossil record in their chemical composition (see e.g., the review by Gratton et al., 2012). Photometrically, GCs often exhibit spread, split and even multiple sequences that can be explained by different chemical composition among cluster stars, in particular of light elements like He, C, N, O (e.g., Carretta et al., 2011b; Sbordone et al., 2011; Milone et al., 2012a; Piotto et al., 2015). Our FLAMES survey of more than 20 Milky Way (MW) GCs (see Carretta et al., 2009a, 2014b, and references therein) combined with literature data, demonstrated that most, perhaps all, GCs host multiple stellar populations (see Carretta et al., 2010a). Variations of Na and O (and

sometimes of Mg and Al) abundances trace these different sub-populations.

Our large and homogeneous database allowed us a quantitative study of the Na-O anticorrelation. In all the analyzed GCs we found about one third of stars of primordial composition, similar to that of field stars of similar metallicity (low Na, high O), i.e., belonging to the first generation (FG). The other two thirds have a modified composition (increased Na, depleted O) and belong to the second generation (SG) of stars, polluted by the FG (see, e.g., Carretta et al., 2009a,b). Which were the more massive stars of FG that produced the gas of modified composition is still an unsettled question, see e.g., Decressin et al. (2007); Ventura et al. (2001), or Bastian et al. (2013) for an alternative view.

We also found that the extension of the Na-O anticorrelation tends to be larger for higher mass GCs and that, apparently, there is an observed minimum cluster mass for appearance of the Na-O anticorrelation (Carretta et al., 2010a). It is important to understand if this limit is due to the small statistics (less low-mass clusters have been studied, and only a few stars were observed in each). This is an important constraint for cluster formation mechanisms, because it indicates the mass at which we expect that a cluster is able to retain part of the ejecta of the

Send offprint requests to: A. Bragaglia, angela.bragaglia@oabo.inaf.it

* Based on observations collected at ESO telescopes under programme 093.B-0583 and on data obtained from the ESO Science Archive Facility under request number 94403

** Tables xx, yy, and zz are only available in electronic form at the CDS via anonymous ftp to cdsarc.u-strasbg.fr (130.79.128.5) or via <http://cdsweb.u-strasbg.fr/cgi-bin/qcat?J/A+A/???/???>

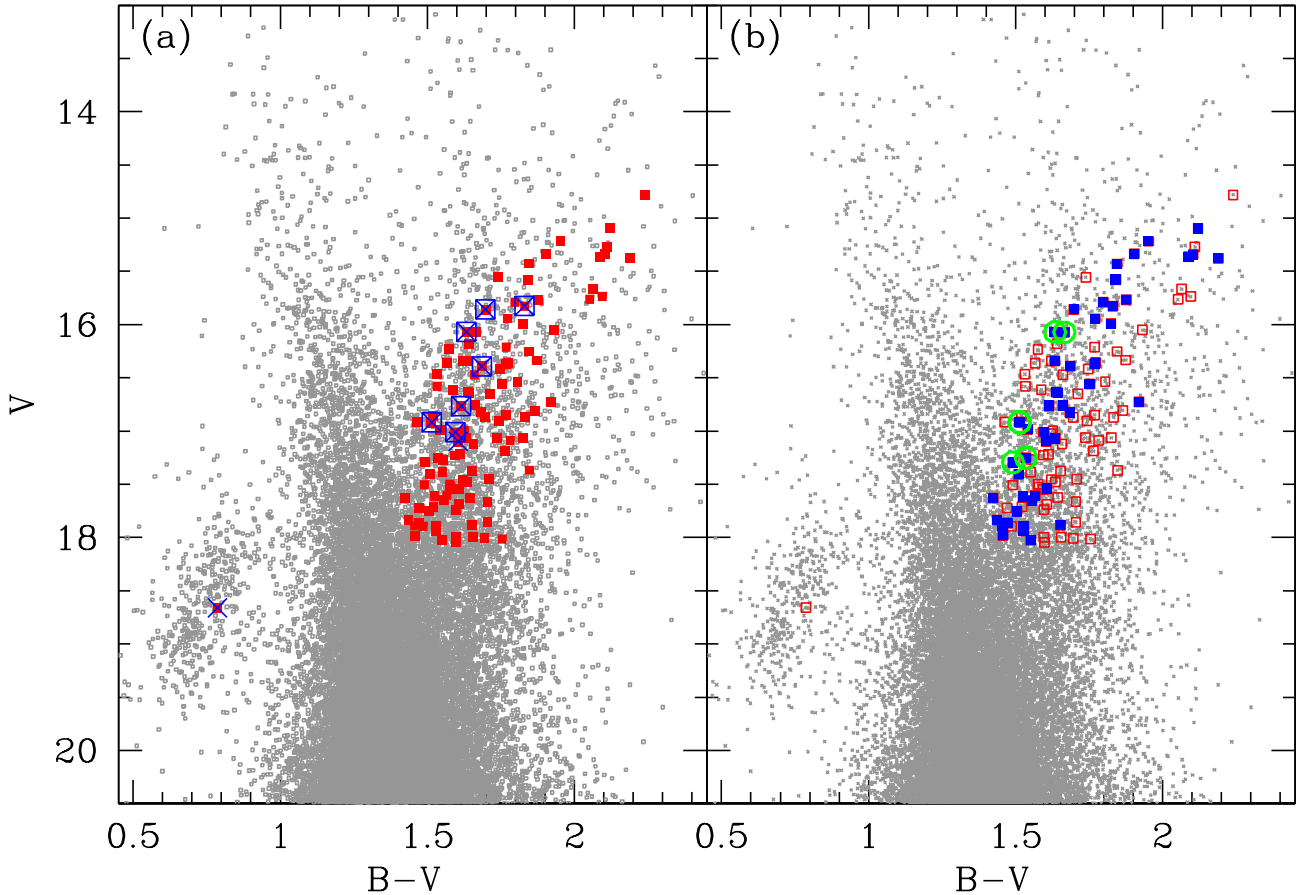


Fig. 1. (a) CMD of NGC 6139, with its quite short blue HB. In grey all stars, in red all targets observed with FLAMES. The seven UVES stars are indicated by blue open squares; the stars with RV from Saviane et al. (2012) by blue crosses. (b) The non member stars (and the star on the HB) are indicated by red open squares, the stars candidate members on the basis of their RV by filled blue squares. The member stars define a reasonably tight RGB and we indicate with green circles the probable AGB stars (see Sec. 3.1)

FG, hence to show the Na-O signature (the masses of the original clusters are expected to be much higher than the present ones, since the SG has to be formed by the ejecta of the FG).

Variations in Na, O, and He are tied, but do not tell us exactly the same story. The effects of increased He are visible in colour-magnitude diagrams (CMD) in the main sequence (MS) phase (e.g., Piotto et al., 2007) or, more evidently, in the horizontal branch phase (HB, e.g., D’Antona et al. 2005; Gratton et al. 2010; Milone et al. 2014). Based on the possibility of reproducing their HBs with a single He value, Caloi & D’Antona (2011), proposed that some GCs are composed by a single generation (FG-only) or predominantly by a single generation (mainly-FG). It would be important to measure their Na, O, and Al abundances to clarify the issue. In fact Al, produced only at higher temperatures than Na

(e.g., Prantzos et al., 2007, for an application to the GC peculiar chemistry), i.e. by more massive stars, should follow the He enrichment better than Na (and O). We can then expect to find Na and O variations without significant He enhancement; this would produce short HBs (and no variations in Al).¹ This is what seems to happen, for instance, for NGC 6397 and NGC 6838 (Carretta et al., 2009b), for which Gratton et al. (2010) found no necessity of He dispersion to explain their HBs. However, Milone et al. (2012b), studying the main sequence of NGC 6397, found an internal variation in Y of about 0.01, small, but exceeding their measurement error. In summary, we would be in presence of FG and SG stars even without significant He variations; this is important to understand the cluster formation and early intracluster gas pollution.

¹ T

After studying the high-mass clusters, we begun a systematic study of low-mass GCs, FG-only/mainly GCs, and high-mass and old open clusters (OCs). Our goal is to empirically find the mass limit for the appearance of the Na-O anticorrelation and to ascertain whether there are differences between high-mass and low-mass clusters' properties, e.g. in the relative fraction of FG and SG stars.

We also included GCs belonging to the Sagittarius dwarf spheroidal (Sgr dSph) to study if there are differences in GCs formed in different environments (the MW and dwarf galaxies). In fact, GCs born in a dSph are expected to have experienced a milder tidal field thus possibly retaining a larger fraction of their original mass. Only a few old GCs in Fornax and LMC have their abundances derived using high-res spectroscopy. These GCs also seem to host two populations (Letarte et al., 2006; Johnson et al., 2006; Mucciarelli et al., 2009) but the fractions of FG and SG stars in Fornax and LMC GCs of similar mass seem different. Is this again a problem of low statistics or is the galactic environment (a dwarf spheroidal vs a dwarf irregular) influencing the GC formation mechanism? This is outside the main theme of the present paper and we refer the interested reader to the papers by Larsen et al. (2012); D'Antona et al. (2013) for a more detailed discussion.

We have already gathered high-resolution spectra of a low-mass GC (NGC 6535, which will be analysed in a forthcoming paper), two high-mass OCs (Berkeley 39, NGC 6791, see Bragaglia et al. 2012, 2014), a proposed FG-only GC (NGC 6139, this paper), and Terzan 8 (Carretta et al., 2014a), belonging to the Sgr dSph. In Terzan 8 we see some indication of a SG, at variance with other low-mass Sgr GCs (Ter 7, Pal 12 Tautvaišienė et al. 2004; Sbordone et al. 2007; Cohen 2004) or to Rup 106 (Villanova et al., 2013). However, in Terzan 8 the SG seems to be a minority component, contrary to what occurs for high-mass GCs. The Na-O anticorrelation had never been observed in OCs (de Silva et al., 2009; MacLean et al., 2014) and we confirmed this using large samples of stars both for Berkeley 39 (Bragaglia et al., 2012) using FLAMES spectra and NGC 6791 (Bragaglia et al., 2014) using Hydra@WIYN and HIRES@Keck spectra. In particular, for NGC 6791, where Geisler et al. (2012) claimed to have found some variations in Na, O, we did not detect any evidence of this trend. Our findings are corroborated by independent works, see Cunha et al. (2015); Boesgaard et al. (2015).

We concentrate here on the possibly FG-only cluster NGC 6139. In Section 2 we present literature information on the cluster, in Section 3 we describe the photometric data, the spectroscopic observations, and the derivation of atmospheric parameters. The abundance analysis is presented in Section 4 and a discussion on the light-element abundances is given in Section 5.

2. NGC 6139 in literature

NGC 6139 is a massive GC (its absolute visual magnitude, a proxy for mass, is $M_V = -8.36$, Harris 1996) located toward the centre of the MW, at $l = 342.37^\circ$, $b = 6.94^\circ$. The cluster has received relatively scarce attention in the past; in particu-

lar, it has never been studied with high-resolution spectroscopy before.

Hazen (1991) found ten variable stars in NGC 6139, five of which are RR Lyrae stars. The four RRab seem to indicate a Oosterhoff type II. A colour-magnitude diagram (CMD) was presented by Samus' et al. (1996); they employed photographic *B* and *V* plates and their photometry reaches only the red giant branch (RGB) and HB. They found the cluster quite metal-poor (close to $[\text{Fe}/\text{H}]=-2$) from the slope of the RGB, and highly reddened. Zinn & Barnes (1998) used *VI* photometry barely reaching the main sequence turn-off, noted the high and differential reddening (and corrected for a gradient), and determined $[\text{Fe}/\text{H}]=-1.71 \pm 0.20$ and a mean reddening of $E(V-I) = 1.03 \pm 0.04$, corresponding to $E(B-V) = 0.76 \pm 0.03$. Similar results were reached by Ortolani et al. (1999) on the basis of *VI* photometry and Davidge (1998) who used near-infrared data and who also noted that the differential reddening is not a significant problem, since the RGB sequence becomes very well defined once the field stars contamination is statistically removed. Finally, Piotto et al. (2002) presented WFPC2 photometry, as part of their HST snapshot programme (74 MW GCs observed with the *F439W* and *F555W* bands) the RGB and HB are very well defined, and the main sequence turn-off is better defined than in previous works. Their data are publicly available and we used them for the present work (see next Section)

The only determination of metallicity based on spectroscopy is by Saviane et al. (2012), who used spectra at resolution $R \sim 2500$ in the region of the infrared Ca II triplet (CaT). NGC 6139 is one of the 20 GCs in the paper. They observed 19 stars, 15 of which were considered members (we used this information to select our targets, see next Section). The metallicity they obtained from the CaT lines is $[\text{Fe}/\text{H}]=-1.63$, rms=0.13 (on the metallicity scale defined in Carretta et al. 2009c).

Caloi & D'Antona (2011) include NGC 6139 among their list of candidate FG clusters. They tried to identify those clusters whose HB could be reproduced by a single mass (in the framework where the dispersion in mass of HB stars is due - at least in part - to variations in He content, in turn indication of multiple generations). A first clue is the short HB (similar to the HB of NGC 6397, see Piotto et al. 2002, which, however has both a "normal" Na-O anticorrelation, and a small ΔY , see Carretta et al. 2009a,b; Milone et al. 2012b, respectively). However, given the high mass ($\log M = 5.58 M_\odot$, their Table 1), NGC 6139 should have produced a SG, but failed to lose a large fraction of the FG stars, so it should be presently FG-dominated. Caloi & D'Antona (2011) do not discuss in detail the case for NGC 6139, but its inclusion in the list, combined with the absence of previous high-resolution spectroscopic studies made it a good target for our on-going programme.

3. Observations and analysis

Of the photometric data discussed in previous section, only the HST catalogue is publicly available. However, the very small field of view (FoV, about 2' side) is not well suited to the

Table 1. Log of FLAMES observations.

Setup	UT Date (yyyy-mm-dd)	UT _{init} (hh:mm:ss)	exptime (s)	airmass	seeing (arcsec)
HR11	2014-05-10	02:25:58.027	3600	1.459	0.76
HR11	2014-05-10	03:27:50.586	3600	1.217	0.88
HR11	2014-05-10	04:29:58.656	3600	1.091	0.64
HR11	2014-05-10	05:36:41.844	3600	1.035	0.68
HR11	2014-05-10	06:50:54.214	3600	1.052	0.57
HR11	2014-05-10	07:54:38.745	3600	1.136	0.47
HR13	2014-07-22	03:21:00.913	3600	1.164	1.06
HR13	2014-07-22	04:24:36.587	3600	1.366	1.09
HR13	2014-07-25	03:14:57.248	3600	1.178	0.76
HR13	2014-07-26	04:12:36.160	3600	1.383	0.59
HR21	2014-06-03	01:01:28.004	3090	1.409	0.86
HR21	2014-07-03	00:29:34.582	3090	1.137	0.99

FLAMES FoV (25' diameter). We then retrieved from the ESO archive some *B* and *V* filter frames acquired (under program 68.D-0265) with the Wide Field Imager (WFI) at the 2.2m ESO-MPG telescope, which has a FoV of about 30' side.

They were reduced in the standard way, correcting for bias and flat field using IRAF.² Stars were detected independently on the *B* and *V* frames and the instrumental magnitudes were obtained using the Point Spread Function (PSF) fitting code DAOPHOT-II/ALLSTAR (Stetson, 1987, 1993). We employed the 2 *Micron All Sky Survey* Catalogue (2MASS, Skrutskie et al. 2006) and the CataXcorr code³, developed by P. Montegriffo, to compute the astrometric solution and transform the instrumental pixel coordinates into J2000 celestial coordinates. The astrometric precision is about 0.2 arcsec, perfectly compatible with the requirements of the FLAMES observations. No standard stars were available, so we calibrated our photometry to the HST one using the stars in common. The final photometric catalogue will be made available through the CDS.

The resulting CMD is shown in Fig. 1. As expected from its Galactic position, the field stars contamination is conspicuous, but the cluster RGB and HB are visible, especially when restricting to the very central region. The cluster sequences are also affected by differential reddening (DR), as already discussed in literature. This could be relevant for the spectroscopic analysis, since our atmospheric parameters are derived from photometry. However, as already done for other difficult cases, resorting to optical-IR colours (in particular, $V - K$), greatly alleviates the problem. For instance, the bulge GC GC 6441 (Gratton et al., 2007) has an rms scatter of 0.05 mag in $E(B - V)$, resulting in a random (star-to-star) uncertainties in the effective temperatures of ± 80 K. We roughly evaluated the size of DR for NGC 6139 by defining a red giant branch (RGB) ridge line with the help of the HST photometry and projecting the candidate members (see next section) on it along the reddening

² IRAF is distributed by the National Optical Astronomical Observatory, which are operated by the Association of Universities for Research in Astronomy, under contract with the National Science Foundation.

³ <http://www.bo.astro.it/~paolo/Main/CataPack.html>

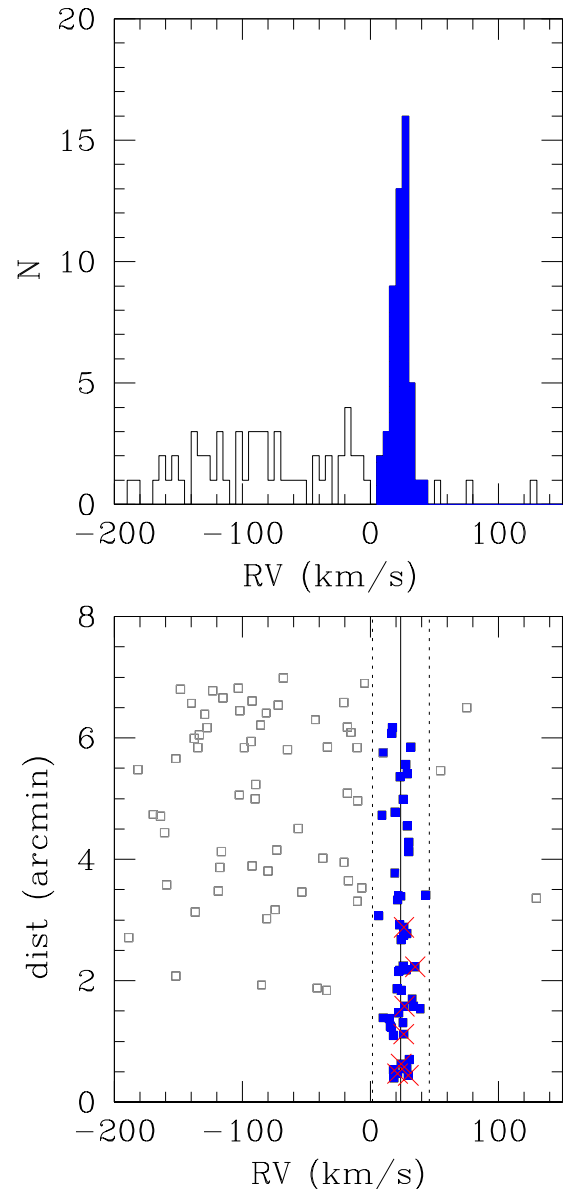


Fig. 2. Upper panel: histogram of all measured RVs (open histogram) and of the candidate member stars only (blue filled histogram). Lower panel: RVs versus distance from the cluster centre. The candidate member stars are indicated by filled blue squares, the UVES targets by large red crosses, while the lines indicate the cluster mean RV and the $\pm 3\sigma$ interval.

vector. The average displacement required is 0.03 mag so we expect a possible error of the order of 50 K.

3.1. FLAMES spectra

NGC 6139 was observed with the multi-object spectrograph FLAMES@VLT (Pasquini et al., 2002). We used the GIRAFFE high-resolution setups HR11, HR13, and HR21 ($R=24200, 22500, 16200$, respectively) which contain two Na doublets, the [O I] line at 6300 Å, and the Al doublet at 8772 Å, plus several Mg lines. The observations were performed in ser-

vice mode; a log is presented in Table 1. The HR11 and HR13 GIRAFFE observations were coupled with the high-resolution ($R=47000$) UVES 580nm setup ($\lambda\lambda \simeq 4800 - 6800 \text{ \AA}$) and the HR21 observations with the UVES 860nm setup ($\lambda\lambda \simeq 6600 - 10600 \text{ \AA}$). We will use only the 580nm spectra in this paper, for uniformity with our previous works and because they have better signal to noise.

The B, V WFI catalogue was used to select candidate targets for the spectroscopic observations. As done for all other GCs in our sample, we chose only stars without close neighbours ($\leq 2.5''$). We cross-identified the stars in Saviane et al. (2012) to allocate seven UVES fibres to high probability cluster members; the eighth fibre was put on an empty spot for sky subtraction. We allocated 103 GIRAFFE fibres to RGB stars, one to a HB star, and 16 to sky positions. Virtually all targets are brighter than the RGB bump ($V = 17.867 \pm 0.019$; Nataf et al. 2013). The 111 stars observed are shown in Fig. 1(a) with different symbols; their coordinates and magnitudes are given in Table 2 (for candidate members, based on their RV) and Table 3 (for non members). All stars observed are within 7 arcmin from the centre, see Fig. 2, lower panel, i.e., well within the tidal radius (10.5 arcmin, Harris 1996). Almost all stars observed are beyond the half-mass radius (0.85 arcmin, Harris).

The spectra were reduced using the ESO pipelines for UVES-FIBRE and GIRAFFE data; they take care of bias and flat field correction, order tracing, extraction, fibre transmission, scattered light, and wavelength calibration. We then used IRAF routines on the 1-d, wavelength-calibrated individual spectra to subtract the (average) sky, shift to zero RV, and combine all the exposures for each star. The region near the [O I] line required special attention because of the strong sky emission and the many absorptions. Given the low RV of the cluster, the HR13 exposures were scheduled when the Earth motion took the sky emission farther away from the stars' [O I] line. We further checked that in all these exposures the telluric absorptions did not fall on the stars' line, by visual comparison with a telluric template. The RV was measured using DOOp (Cantat-Gaudin et al., 2014), an automated wrapper for DAOSPEC (Stetson & Pancino, 2008); the average, heliocentric value for each star is given in Tables 2 and 3.

We show in Fig. 2 the histogram of the RVs and a plot of RVs versus distance from cluster centre (taken by Harris 1996, 2010 web update); the cluster signature is clear. Our is the first estimate of RV based on a large number of stars observed at high-resolution; we found $\langle RV \rangle = +28.88$, $\text{rms}=7.34 \text{ km s}^{-1}$ (a typical rms, for a GC). This value is compatible with the $RV=6.7\pm 6.0 \text{ km s}^{-1}$ in Harris (1996), based on much lower resolution and quality data⁴, and is in good agreement with Saviane et al. (2012), who give $RV=34\pm 4 \text{ km s}^{-1}$, based on 15 stars (for a direct comparison of RVs for eight stars in common, see Table 2).

We are left with 50 candidate members based on the RV, i.e., falling within $\pm 3\sigma$ of the cluster average. After pruning the sample, the RGB of NGC 6139 is well defined and tight,

even in presence of DR (see Fig. 1(b)). In the following we will discuss only them.

Following our well tested procedure (for a lengthy description, see e.g., Carretta et al., 2009a,b), effective temperatures T_{eff} for our targets were derived using an average relation between apparent magnitudes and first-pass temperatures from $V-K$ colours and the calibrations of Alonso et al. (1999, 2001). This method permits to decrease the star-to-star errors in abundances due to uncertainties in temperatures, since magnitudes are less affected by uncertainties than colours. This is particularly true for NGC 6139, which presents high and variable reddening, for which we used the apparent K magnitudes in our relation with T_{eff} because the impact of the DR on these magnitudes is smaller. The adopted reddening $E(B-V) = 0.75$ and distance modulus $(m-M)_V = 17.35$ are from the Harris (1996) catalogue. Gravities were obtained from apparent magnitudes and distance modulus, assuming the bolometric corrections from Alonso et al. (1999). We adopted a mass of $0.85 M_{\odot}$ for all stars and $M_{\text{bol},\odot} = 4.75$ as the bolometric magnitude for the Sun, as in our previous studies.

We eliminated trends in the relation between abundances from Fe I lines and expected line strength (Magain, 1984) to obtain values of the microturbulent velocity v_t .

Finally, using the above values we interpolated within the Kurucz (1993) grid of model atmospheres (with the option for overshooting on) to derive the final abundances, adopting for each star the model with the appropriate atmospheric parameters and whose abundances matched those derived from Fe I lines. Five stars among the candidate members turned out to have a metallicity higher by more than 0.5 dex than the average of the others; they are probably field stars and have been excluded from the most secure sample of RV *and* metallicity members. The atmospheric parameters for all bona fide member stars are given in Table 4.

Six of the candidate members (two with UVES and four with GIRAFFE spectra) turned out too metal-poor (by about 0.15 dex); their position in the CMD seemed to indicate that they could be Asymptotic Giant Branch stars (AGB) and not RGB. Following the same procedure used for the RGB stars, we derived a separate colour-temperature relation for them, finding temperatures higher by about 110 K. Adopting the new temperatures we repeated the analysis, finding a metallicity in very good agreement with the cluster average. These second values for T_{eff} and metallicity are given in Table 4.

4. Abundances

Beside Fe, we present here abundance of O, Na, Mg, and Al. The last was derived from the Al I doublet at 6696-98 \AA for stars observed with UVES, and from the doublet at 8772 \AA for stars observed with GIRAFFE. The abundance ratios for all elements are given in Table 5, together with number of lines used and rms scatter.

The abundances were derived using equivalent widths (EW). We measured the EW of iron and other elements using the code ROSA (Gratton, 1988) adopting a relationship between EW and FWHM (for details, see Bragaglia et al. 2001). The atomic data for all the lines in the UVES spectra and in the

⁴ Harris (1996) refers to Webbink (1981), who uses RVs from Kinman (1959), derived on spectra at $R \sim 200$ of four stars.

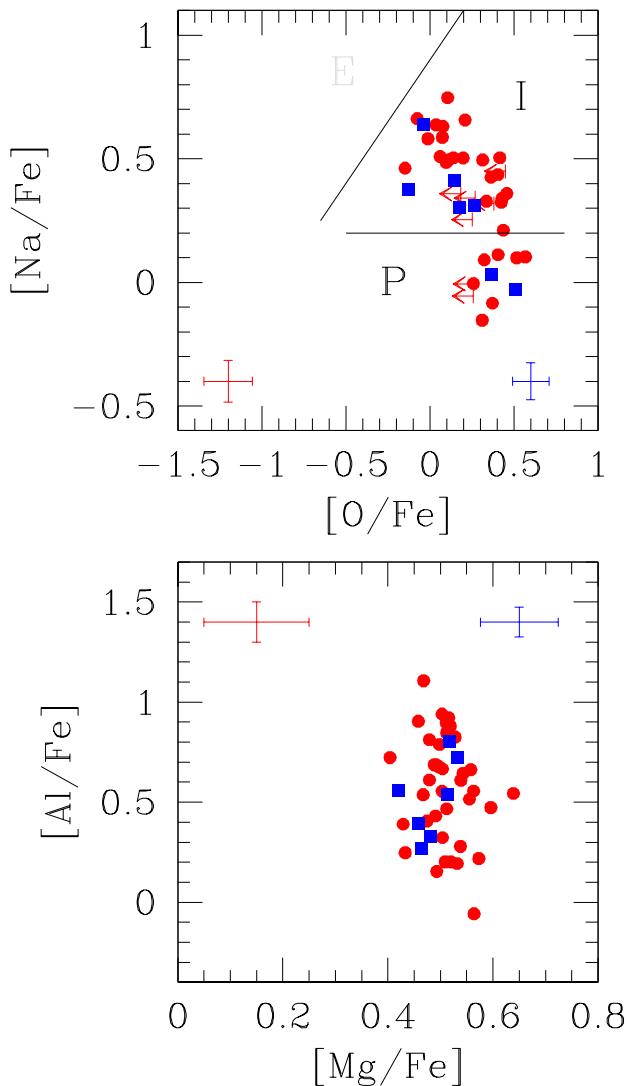


Fig. 3. Anticorrelations between light elements: Na-O (upper panel) and Mg-Al (lower panel). GIRAFFE stars are indicated by red filled circles and UVES stars by filled blue squares; upper limits in O are shown as arrows. The errorbars are the cluster average internal (star-to-star) errors for each element for the GIRAFFE sample in red and UVES in blue (see text). In the upper panel we indicate the separation between P and I, and I and E populations, according to Carretta et al. (2009a).

HR11, HR13 setups and the solar reference values come from Gratton et al. (2003). The Na abundances were corrected for departure from local thermodynamical equilibrium according to Gratton et al. (1999).

The derived Fe abundances do not show any trend with T_{eff} . The average metallicity derived from stars with UVES spectra is $[\text{Fe}/\text{H}] = -1.579 \pm 0.015 \pm 0.058$ (rms = 0.040 dex, 7 stars) from neutral species, where the first error is from statistics and the second is systematic (see below for the computation). For stars with GIRAFFE spectra we found a very similar value: $[\text{Fe}/\text{H}] = -1.596 \pm 0.006 \pm 0.042$ (rms = 0.038 dex, 38 stars). The abundance derived from single ionized species is in very good

agreement. We found $[\text{Fe}/\text{H}]_{\text{I}} = -1.541 \pm 0.016 \pm 0.054$ (rms = 0.043 dex, 7 stars) and $[\text{Fe}/\text{H}]_{\text{II}} = -1.579 \pm 0.008 \pm 0.042$ (rms = 0.048 dex, 38 stars) for UVES and GIRAFFE, respectively. This supports the adopted temperature scale and gravities.

Ours is the first high-resolution spectroscopic study of this cluster, so no real comparison with previous determinations is possible. However, the metallicity we find is in good agreement with the one based on CaT ($[\text{Fe}/\text{H}] = -1.63$, Saviane et al. 2012) and with the general finding of a low metallicity (~ -1.7 or -2) based on photometry.

To estimate the error budget we closely followed the procedure described in Carretta et al. (2009a,b). Table 6 (for UVES spectra) and Table 7 (for GIRAFFE spectra) provide the sensitivities of abundance ratios to errors in atmospheric parameters and EWs and the internal and systematic errors. For systematic errors we mean the errors that are different for the various GCs considered in our series and which produce scatter in relations involving different GCs; however, they do not affect the star-to-star scatter in NGC 6139. The cluster uncertainty in T_{eff} can be estimated by multiplying the slope of the relation $T_{\text{eff}} - (V - K)$ in NGC 6139 and the uncertainty in $E(V - K)$ (assumed to be 0.055 mag). We also quadratically sum a contribution from a conservative estimate of 0.02 mag error in the zero point of $V - K$ colour. The resultant uncertainty is propagated together with those in distance modulus and stellar mass to estimate the systematic uncertainty in surface gravity, while the systematic error in v_t is simply obtained by dividing the internal error for the square root of the number of stars. The cluster (systematic) error in the metallicity for NGC 6139 is then obtained by the quadratic sum of the above three terms (multiplied for the proper sensitivity) with the statistical errors of individual abundance determination. The sensitivities were obtained by repeating the abundance analysis for all stars, while changing one atmospheric parameter at the time, then taking the average; this was done separately for UVES and GIRAFFE spectra. The amount of change in the input parameters used in the sensitivity computations is given in the Table header.

5. Light elements anti-correlations

Our final sample consists of 45 giant stars (seven observed with UVES and 38 with GIRAFFE, no stars are in common). We could measure Na, Mg, and Al in all spectra (UVES and GIRAFFE), while O was measured in all seven UVES stars but only in 36 GIRAFFE stars (29 actual detection and seven upper limits).

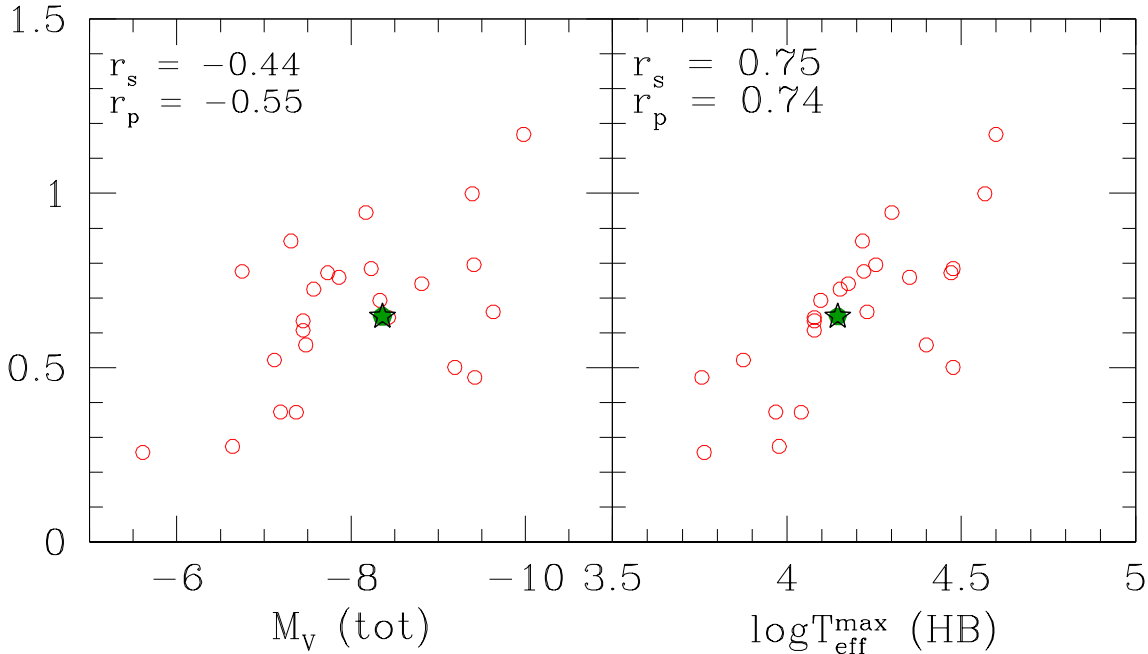
The resulting relations between O and Na, Mg and Al are shown in Fig. 3, where we clearly see the normal pattern of light elements abundance ratios in GCs. NGC 6139 displays a Na-O anticorrelation like all massive GCs studied to date. Interestingly, it also shows a large variation in Al coupled with a moderate variation in Mg. A variation in Al is not seen in all GCs (see Fig. 6 in Carretta et al., 2009b); however, also when Al varies the moderate variation in Mg is typical, with only rare exceptions such as e.g., NGC 2808, NGC 6752 (Carretta, 2014; Carretta et al., 2012). On the other hand, we observe a clear Na-Al correlation, with a Pearson correlation coefficient $r_p = 0.70$, which is very significant. This confirms that the Na-

Table 6. Sensitivities of abundance ratios to variations in the atmospheric parameters and to errors in the equivalent widths, and errors in abundances for stars of NGC 6139 observed with UVES.

Element	Average n. lines	T_{eff} (K)	$\log g$ (dex)	[A/H] (dex)	v_t kms $^{-1}$	EWs (dex)	Total Internal	Total Systematic
Variation		50	0.20	0.10	0.10			
Internal		4	0.04	0.04	0.06	0.01		
Systematic		46	0.06	0.06	0.02			
[Fe/H] _I	86	+0.060	-0.002	-0.008	-0.028	0.011	0.021	0.058
[Fe/H] _{II}	16	-0.031	+0.086	+0.022	-0.014	0.026	0.034	0.042
[O/Fe] _I	1	-0.044	+0.084	+0.038	+0.027	0.104	0.108	0.096
[Na/Fe] _I	2	-0.016	-0.038	-0.015	+0.022	0.074	0.075	0.088
[Mg/Fe] _I	2	-0.016	-0.009	-0.000	+0.012	0.074	0.074	0.021
[Al/Fe] _I	2	-0.017	-0.008	-0.002	+0.026	0.074	0.075	0.077

Table 7. Sensitivities of abundance ratios to variations in the atmospheric parameters and to errors in the equivalent widths, and errors in abundances for stars of NGC 6139 observed with GIRAFFE.

Element	Average n. lines	T_{eff} (K)	$\log g$ (dex)	[A/H] (dex)	v_t kms $^{-1}$	EWs (dex)	Total Internal	Total Systematic
Variation		50	0.20	0.10	0.10			
Internal		4	0.04	0.04	0.13	0.02		
Systematic		46	0.06	0.05	0.02			
[Fe/H] _I	35	+0.058	-0.001	-0.007	-0.025	0.022	0.041	0.054
[Fe/H] _{II}	2	-0.035	+0.088	+0.020	-0.007	0.067	0.101	0.042
[O/Fe] _I	1	-0.041	+0.081	+0.034	+0.023	0.095	0.144	0.053
[Na/Fe] _I	3	-0.016	-0.040	-0.018	+0.017	0.067	0.084	0.043
[Mg/Fe] _I	2	-0.021	-0.009	-0.003	+0.013	0.095	0.100	0.021
[Al/Fe] _I	2	-0.030	-0.006	-0.002	+0.019	0.095	0.101	0.051

**Fig. 4.** Left-hand panel: correlation between total absolute magnitude and the interquartile range of the [O/Na] ratio for GC in our FLAMES survey (Carretta et al., 2009a, 2010b, 2011a, 2013b, 2014b, 2015, and references therein). Right-hand panel: relation between the maximum temperature along the HB (Recio-Blanco et al., 2006; Carretta et al., 2007) and IQR[O/Na]. In each panel NGC 6139 indicated by a filled green star. The Spearman rank correlation coefficient r_s and the Pearson linear correlation coefficient r_p are listed in each panel.

Na and Mg-Al cycles are related, but also suggests that they do not occur exactly in the same polluting stars.

Using the criteria defined in Carretta et al. (2009a) we can define the fraction of stars belonging to the primordial (P) and second-generation (I, E) components. The fraction of first-generation P stars is $26\% \pm 8\%$; the fraction of second-generation I stars (with moderate modification of the abundances) is $74\% \pm 13\%$; finally, there are no second-generation E stars (with extremely modified composition) in our sample of 43 stars in NGC 6139. These numbers agree with what is found in all massive Milky Way GCs (see e.g., Carretta et al., 2010a, 2014b; Johnson & Pilachowski, 2012, and references therein); SG stars are presently the dominant population in them. Our study then does not confirm NGC 6139 as a mainly-FG cluster, as proposed by Caloi & D’Antona (2011).

As it happened for the other GCs in our sample (e.g., Carretta et al., 2009a), where most of the abundance ratios are based on GIRAFFE spectra, the errors on abundances produce almost continuous distributions (Fig. 3). However, a separation between the P and I stars is visible in the upper panel (Na and O), especially for the stars observed with UVES. A clearcut separation in groups along the Na-O anticorrelation has been seen only in high-quality and resolution data, such as the UVES spectra in M4 (Marino et al., 2008) and NGC 2808 (Carretta, 2014). The Mg-Al distribution (Fig. 3 lower panel) looks continuous, with a total excursion of about 1 dex in [Al/Fe].

The Na-O anticorrelation has moderate extension, with an interquartile range for the [O/Na] ratio (Carretta, 2006) $\text{IQR}[\text{O}/\text{Na}] = 0.647$. This IQR makes NGC 6139 fit in the relations with absolute magnitude (M_V , i.e., mass) and maximum temperature reached on the HB ($T_{\text{eff}}^{\text{max}}(\text{HB})$, Recio-Blanco et al. 2006; Carretta et al. 2007, see Fig. 4 for a graphical representation).

In conclusion, with our study of 45 member stars in NGC 6139 conducted with FLAMES spectra we determined for the first time its metallicity with high-resolution spectroscopy (the cluster has an intermediate metallicity, with $[\text{Fe}/\text{H}] = -1.58$ dex). We also measured the light elements O, Na, Mg, and Al involved in proton-capture reactions of H-burning at high temperatures; we detected the usual correlations and anticorrelations found in almost all GCs investigated so far. The ratio of first-to-second generation stars in NGC 6139 is typical of the majority of GCs and is consistent with its relatively high total present-day mass. We do not support the idea that NGC 6139 is a FG-dominated cluster. The intermediate extension of the Na-O anticorrelation, as measured by the interquartile range of the [O/Na] ratio, fits very well the relation with the maximum temperature along the HB found by Carretta et al. (2007). All in all NGC 6139 behaves like a normal MW GC of similar mass and HB extension. The formation event that shaped its internal chemistry seems consistent with the pattern of a regular, relatively high-mass, blue HB GC.

However, the finding of a large variation in Al, which should also imply some spread in He, does not perfectly fit with the HB of the cluster. We calculated $\text{IQR}[\text{Al}/\text{Mg}]$, finding a value of 0.425; according to Fig. 28 in Gratton et al. (2010), this would require a ΔY of about 0.02 (but note that the relation between $\text{IQR}[\text{Al}/\text{Mg}]$ and ΔY is rather poorly determined,

being based on only eight points). We note that also the more massive, metal-poorer NGC 5024 (M53, with $M_V = -8.71$, $[\text{Fe}/\text{H}] = -2.10$, Harris 1996), proposed as a FG-dominated GC by Caloi & D’Antona (2011) on the basis of its HB and discussed at length in that paper, has been demonstrated to host a substantial SG by Mészáros et al. (2015), using APOGEE data. NGC 5024 has a large spread in Al (with a bimodal distribution) and almost no Mg variation; it behaves like NGC 5272 (M3, $M_V = -8.88$, $[\text{Fe}/\text{H}] = -1.50$, Harris 1996), another GC with a rather short HB, even more massive than NGC 6139, but with a similar metallicity. The relation between Al and He is evidently not completely understood. As an additionally cautionary note, Bastian et al. (2015) claim that no one of the enrichment mechanisms proposed to explain multiple populations in GCs can consistently do so, because all predict too large He spreads in order to reproduce the observed spreads in light elements, notably those in Na and O. More observational constraints are required, both from spectroscopy with large samples of stars for which elements of all nucleosynthetic chains are measured (like we and other groups are doing for an increasing number of GCs) and from precise photometry (e.g., Piotto et al., 2015, to determine He). These constraints will be helpful to improve modelling the formation and early enrichment phases of GCs.

Acknowledgements. We thank the referee for constructive comments which improved the paper. This research has made use of WEBDA, SIMBAD database, operated at CDS, Strasbourg, France, and NASA’s Astrophysical Data System. This publication makes use of data products from the Two Micron All Sky Survey, which is a joint project of the University of Massachusetts and the Infrared Processing and Analysis Center/California Institute of Technology, funded by the National Aeronautics and Space Administration and the National Science Foundation. This research has been partially funded by PRIN INAF 2011 “Multiple populations in globular clusters: their role in the Galaxy assembly”, and PRIN MIUR 2010-2011, project “The Chemical and Dynamical Evolution of the Milky Way and Local Group Galaxies”.

References

- Alonso, A., Arribas, S., & Martínez-Roger, C. 1999, *A&AS*, 140, 261
- Alonso, A., Arribas, S., & Martínez-Roger, C. 2001, *A&A*, 376, 1039
- Bastian, N., Lamers, H. J. G. L. M., de Mink, S. E., et al. 2013, *MNRAS*, 436, 2398
- Bastian, N., Cabrera-Ziri, I., & Salaris, M. 2015, *MNRAS*, 449, 3333
- Boesgaard, A. M., Lum, M. G., & Deliyannis, C. P. 2015, *ApJ*, 799, 202
- Bragaglia, A., Carretta, E., Gratton, R. G., et al. 2001, *AJ*, 121, 327
- Bragaglia, A., Gratton, R. G., Carretta, E., et al. 2012, *A&A*, 548, AA122
- Bragaglia, A., Sneden, C., Carretta, E., et al. 2014, *ApJ*, 796, 68
- Caloi, V., & D’Antona, F. 2011, *MNRAS*, 417, 228

- Cantat-Gaudin, T., Donati, P., Pancino, E., et al. 2014, *A&A*, 562, AA10
- Carretta, E. 2006, *AJ*, 131, 1766
- Carretta, E. 2014, *ApJ*, 795, L28
- Carretta, E., Recio-Blanco, A., Gratton, R. G., Piotto, G., & Bragaglia, A. 2007, *ApJ*, 671, L125
- Carretta, E., Bragaglia, A., Gratton, R. G., et al. 2009a, *A&A*, 505, 117
- Carretta, E., Bragaglia, A., Gratton, R.G., Lucatello, S. 2009b, *A&A*, 505, 139
- Carretta, E., Bragaglia, A., Gratton, R.G., D’Orazi, V., Lucatello, S. 2009c, *A&A*, 508, 695
- Carretta, E., Bragaglia, A., Gratton, R.G., Recio-Blanco, A., Lucatello, S., D’Orazi, V., Cassisi, S. 2010a, *A&A*, 516, 55
- Carretta, E., Bragaglia, A., Gratton, R. G., et al. 2010b, *A&A*, 520, A95
- Carretta, E., Lucatello, S., Gratton, R. G., Bragaglia, A., & D’Orazi, V. 2011a, *A&A*, 533, A69
- Carretta, E., Bragaglia, A., Gratton, R., D’Orazi, V., & Lucatello, S. 2011b, *A&A*, 535, AA121
- Carretta, E., Bragaglia, A., Gratton, R. G., Lucatello, S., & D’Orazi, V. 2012, *ApJ*, 750, L14
- Carretta, E., Gratton, R. G., Bragaglia, A., D’Orazi, V., & Lucatello, S. 2013a, *A&A*, 550, A34
- Carretta, E., Bragaglia, A., Gratton, R. G., et al. 2013b, *A&A*, 557, A138
- Carretta, E., Bragaglia, A., Gratton, R. G., et al. 2014a, *A&A*, 561, AA87
- Carretta, E., Bragaglia, A., Gratton, R. G., et al. 2014b, *A&A*, 564, AA60
- Carretta, E., Bragaglia, A., Gratton, R. G., et al. 2015, *A&A*, 578, A116
- Cohen, J.G. 2004, *AJ*, 127, 1545
- Cunha, K., Smith, V. V., Johnson, J. A., et al. 2015, *ApJ*, 798, L41
- D’Antona, F., Bellazzini, M., Caloi, V., et al. 2005, *ApJ*, 631, 868
- D’Antona, F., Caloi, V., D’Ercole, A., et al. 2013, *MNRAS*, 434, 1138
- Davidge, T. J. 1998, *AJ*, 116, 1744
- Decressin, T., Meynet, G., Charbonnel, C., Prantzos, N., & Ekström, S. 2007, *A&A*, 464, 1029
- Geisler, D., Villanova, S., Carraro, G., et al. 2012, *ApJ*, 756, SL40
- de Silva, G. M., Gibson, B. K., Lattanzio, J., & Asplund, M. 2009, *A&A*, 500, L25
- Gratton, R.G. 1988, *Rome Obs. Preprint Ser.* 29
- Gratton, R. G., Carretta, E., Eriksson, K., & Gustafsson, B. 1999, *A&A*, 350, 955
- Gratton, R. G., Carretta, E., Claudi, R., Lucatello, S., & Barbieri, M. 2003, *A&A*, 404, 187
- Gratton, R., Sneden, C., & Carretta, E. 2004, *ARA&A*, 42, 385
- Gratton, R. G., Lucatello, S., Bragaglia, A., et al. 2007, *A&A*, 464, 953
- Gratton, R. G., Carretta, E., Bragaglia, A., Lucatello, S., & D’Orazi, V. 2010, *A&A*, 517, AA81
- Gratton, R.G., Carretta, E., Bragaglia, A. 2012, *A&A Rev.*, 20, 50
- Harris, W. E. 1996, *AJ*, 112, 1487
- Hazen, M. L. 1991, *AJ*, 101, 170
- Johnson, C. I., & Pilachowski, C. A. 2012, *ApJ*, 754, L38
- Johnson, J. A., Ivans, I. I., & Stetson, P. B. 2006, *ApJ*, 640, 801
- Kinman, T. D. 1959, *MNRAS*, 119, 157
- Kurucz, R. 1993, *ATLAS9 Stellar Atmosphere Programs and 2 km/s grid*. Kurucz CD-ROM No. 13. Cambridge, Mass.: Smithsonian Astrophysical Observatory, 1993., 13,
- Larsen, S. S., Strader, J., & Brodie, J. P. 2012, *A&A*, 544, L14
- Letarte, B., Hill, V., Jablonka, P., et al. 2006, *A&A*, 453, 547
- MacLean, B. T., De Silva, G. M., & Lattanzio, J. 2014, *MNRAS*, 466, 3556
- Magain, P. 1984, *A&A*, 134, 189
- Marino, A. F., Villanova, S., Piotto, G., et al. 2008, *A&A*, 490, 625
- Mészáros, S., Martell, S. L., Shetrone, M., et al. 2015, *AJ*, 149, 153
- Milone, A. P., Piotto, G., Bedin, L. R., et al. 2012a, *ApJ*, 744, 58
- Milone, A. P., Marino, A. F., Piotto, G., et al. 2012b, *ApJ*, 745, 27
- Milone, A. P., Marino, A. F., Dotter, A., et al. 2014, *ApJ*, 785, 21
- Mucciarelli, A., Origlia, L., Ferraro, F. R., & Pancino, E. 2009, *ApJ*, 695, L134
- Nataf, D. M., Gould, A. P., Pinsonneault, M. H., & Udalski, A. 2013, *ApJ*, 766, 77
- Ortolani, S., Bica, E., & Barbuy, B. 1999, *A&AS*, 138, 267
- Pasquini, L., Avila, G., Blecha, A., et al. 2002, *The Messenger*, 110, 1
- Piotto, G., King, I. R., Djorgovski, S. G., et al. 2002, *A&A*, 391, 945
- Piotto, G., Bedin, L. R., Anderson, J., et al. 2007, *ApJ*, 661, L53
- Piotto, G., Milone, A. P., Bedin, L. R., et al. 2015, *AJ*, 149, 91
- Prantzos, N., Charbonnel, C., & Iliadis, C. 2007, *A&A*, 470, 179
- Recio-Blanco, A., Aparicio, A., Piotto, G., de Angeli, F., & Djorgovski, S. G. 2006, *A&A*, 452, 875
- Samus’, N. N., Kravtsov, V. V., Pavlov, M. V., et al. 1996, *Astronomy Letters*, 22, 686
- Saviane, I., da Costa, G. S., Held, E. V., et al. 2012, *A&A*, 540, AA27
- Sbordone, L., Bonifacio, P., Buonanno, R., Marconi, G., Monaco, L., & Zaggia, S. 2007, *A&A*, 465, 815
- Sbordone, L., Salaris, M., Weiss, A., & Cassisi, S. 2011, *A&A*, 534, A9
- Skrutskie, M. F., et al. 2006, *AJ*, 131, 1163
- Stetson, P. B. 1987, *PASP*, 99, 191
- Stetson, P. B. 1993, in Butler C. J., Elliott I., eds, *Stellar photometry - Current techniques and future developments*, Proc. IAU Colloquium 136, Cambridge Univ. Press, Cambridge, p. 291
- Stetson, P. B., & Pancino, E. 2008, *PASP*, 120, 1332
- Tautvaišienė, G., Wallerstein, G., Geisler, D., Gonzalez, G., Charbonnel, C. 2004, *AJ*, 127, 373
- Ventura, P., D’Antona, F., Mazzitelli, I., & Gratton, R. 2001, *ApJ*, 550, L65

- Villanova, S., Geisler, D., Carraro, G., Moni Bidin, C., & Muñoz, C. 2013, *ApJ*, 778, 186
- Webbink, R. F. 1981, *ApJS*, 45, 259
- Zinn, R., & Barnes, S. 1998, *AJ*, 116, 1736

Table 2. Information on the member stars observed. **the complete table is available in the on-line version**

ID	RA (hh:mm:ss)	Dec (dd:pp:ss)	V	B	K (2MASS)	RV (km s ⁻¹)	err (km s ⁻¹)	Notes
UVES								
t00540	16:27:39.82	-38:50:18.05	15.825	17.656	10.601	24.00	0.30	4, RV _{S12} =37
t00553	16:27:39.22	-38:51:18.04	15.859	17.557	10.856	29.63	0.60	1, RV _{S12} =46
t00670	16:27:42.77	-38:50:56.29	16.069	17.703	11.329	21.27	0.50	3, RV _{S12} =36, AGB
t00951	16:27:35.86	-38:53:40.28	16.391	18.077	11.706	26.21	0.60	13, RV _{S12} =44
t01348	16:27:40.82	-38:48:42.10	16.764	18.379	12.049	35.00	0.30	11, RV _{S12} =19
t01554	16:27:38.41	-38:49:23.44	16.920	18.434	12.261	26.71	1.60	8, RV _{S12} =38, AGB
t01699	16:27:42.55	-38:49:53.35	17.010	18.605	12.383	26.09	0.50	7, RV _{S12} =42
GIRAFFE, members								
t00261	16:27:43.32	-38:57:04.20	15.097	17.217	9.530	17.37	0.35	
t00284	16:27:46.06	-38:54:03.74	15.218	17.170	9.988	21.40	0.55	
t00316	16:27:46.75	-38:51:04.61	15.337	17.240	10.145	15.68	0.34	
t00329	16:27:20.70	-38:53:22.86	15.341	17.445	9.744	28.93	0.42	
t00337	16:27:30.42	-38:52:04.70	15.363	17.450	9.754	25.63	0.84	

In Notes we give the number and RV in Saviane et al. (2012);
Star t06169 is on the HB.

Table 3. Information on non member stars on the basis of RV or metallicity, all observed with GIRAFFE. **the complete table is available in the on-line version**

ID	RA (hh:mm:ss)	Dec (dd:pp:ss)	V	B	K (2MASS)	RV (km s ⁻¹)	err (km s ⁻¹)	Note
t00187	16:27:25.45	-38:48:42.66	14.781	17.020	7.078	-16.98	1.00	RV
t00306	16:27:10.97	-38:53:19.81	15.271	17.381	9.388	-85.72	0.49	RV
t00392	16:27:48.91	-38:51:43.38	15.555	17.294	10.639	-34.11	0.99	RV
t00466	16:28:07.92	-38:49:47.99	15.666	17.730	9.262	-181.62	0.69	RV
t00513	16:28:00.26	-38:52:21.00	15.737	17.832	9.739	-116.30	0.48	RV
t00526	16:27:45.67	-38:55:14.59	15.764	17.815	9.802	-160.69	0.52	RV

Table 4. Adopted atmospheric parameters and derived metallicity for confirmed member stars. **the complete table is available in the on-line version**

Star	T _{eff} (K)	log g (dex)	[A/H] (dex)	v _t (km s ⁻¹)	nr	[Fe/H] _I (dex)	rms	nr	[Fe/H] _{II} (dex)	rms
UVES										
t00540	4156	0.95	-1.55	1.85	121	-1.545	0.089	20	-1.551	0.076
t00553	4212	1.07	-1.61	1.40	107	-1.610	0.102	20	-1.505	0.131
t00670	4417	1.28	-1.57	1.43	91	-1.570	0.112	13	-1.566	0.164
t00951	4398	1.44	-1.61	1.93	83	-1.614	0.095	17	-1.475	0.098
t01348	4473	1.57	-1.57	1.52	74	-1.571	0.101	15	-1.586	0.109
t01554	4634	1.76	-1.63	0.98	52	-1.629	0.140	10	-1.588	0.173
t01699	4546	1.72	-1.52	1.64	76	-1.517	0.090	15	-1.517	0.105
GIRAFFE										
t00261	3922	0.51	-1.56	2.09	40	-1.558	0.087	3	-1.524	0.207
t00284	4022	0.71	-1.59	1.97	36	-1.592	0.099	3	-1.517	0.064
t00316	4056	0.77	-1.58	2.03	48	-1.576	0.123	3	-1.576	0.216
t00329	3968	0.59	-1.59	2.02	38	-1.588	0.079	3	-1.514	0.089
t00337	3971	0.59	-1.61	2.08	41	-1.605	0.110	3	-1.512	0.016

Table 5. Light element abundances for confirmed member stars. **the complete table is available in the on-line version**

Star	nr	[O/Fe] _I	<i>rms</i>	nr	[Na/Fe] _I	<i>rms</i>	nr	[Mg/Fe] _I	<i>rms</i>	nr	[Al/Fe] _I	<i>rms</i>	Lim?	PIE
UVES														
t00540	1	-0.041		3	0.637	0.010	3	0.518	0.068	2	0.802	0.008		I
t00553	2	0.174	0.071	3	0.303	0.050	3	0.459	0.038	2	0.395	0.084		I
t00670	1	-0.126		2	0.377	0.089	2	0.420	0.071	2	0.559	0.006		I
t00951	1	0.506		1	-0.028		2	0.482	0.011	2	0.330	0.126		P
t01348	1	0.369		2	0.030	0.055	2	0.464	0.006	1	0.270			P
t01554	1	0.263		2	0.313	0.061	2	0.532	0.204	2	0.724	0.097		I
t01699	1	0.146		2	0.414	0.001	2	0.514	0.102	2	0.536	0.112		I
GIRAFFE														
t00261	2	0.078	0.185	4	0.631	0.040	3	0.503	0.072	2	0.555	0.031		I
t00284	2	0.209	0.006	4	0.657	0.040	3	0.563	0.057	2	0.556	0.000		I
t00316	1	0.037		4	0.637	0.061	2	0.503	0.006	2	0.940	0.128		I
t00329	2	0.430	0.051	4	0.340	0.036	3	0.538	0.015	2	0.279	0.006		I
t00337	2	0.105	0.006	4	0.747	0.019	3	0.516	0.076	2	0.921	0.040		I